Global analysis of nuclear cluster structure from the elastic and inclusive electron scattering

Lei Wang,[1,2] Jian Liu,[2,*] Rensheng Wang,[3,†] Mengjiao Lyu,[4] Chang Xu,[5] and Zhongzhou Ren[1]

[1]*School of Physics Science and Engineering, Tongji University, Shanghai 200092, China*
[2]*College of Science, China University of Petroleum (East China), Qingdao 266580, China*
[3]*School for Radiological and interdisciplinary Sciences (RAD-X), Soochow University, Suzhou 215123, China*
[4]*College of Science, Nanjing University of Aeronautics and Astronautics, Nanjing 210016, China*
[5]*Department of Physics, Nanjing University, Nanjing 210093, China*

(Received 23 October 2020; revised 9 March 2021; accepted 3 May 2021; published 13 May 2021)

Background: Recently, the researches of cluster structure have attracted considerable attention. Many microscopic structure models have been applied to describe the cluster configurations.
Purpose: To better analyze the cluster structure and associate with the experimental observations, comparative studies are carried out in this paper by combining the nuclear structure model with the electron scattering theory.
Method: The density distributions for candidate nuclei of normal and cluster states are obtained from the deformed relativistic Hartree-Bogoliubov (RHB) model. Using some moderate approximations, the corresponding Coulomb form factors $|F_C(q)|^2$ and inclusive cross sections for different configurations are calculated by the distorted wave Born approximation (DWBA) and coherent density fluctuation model (CDFM), respectively.
Results: Comparing the $|F_C(q)|^2$ and inclusive cross sections of different configurations, the effects of nuclear cluster structure can be revealed, due to the differences of nuclear charge radii R_C in coordinate space and the discrepancies of Fermi momentum k_F in momentum space.
Conclusions: Results illustrate that the cluster structure can be reflected from the elastic and inclusive electron scattering. The studies conducted in this paper provide a new approach to analyze the cluster configurations, and are also helpful to guide future electron scattering experiments.

DOI: 10.1103/PhysRevC.103.054307

I. INTRODUCTION

In the past decade, the cluster formation in ground and excited states has been investigated experimentally, providing a new perspective for studying the nuclear structure and nuclear many body problems [1–6]. The mechanism of the cluster formation has attracted a great deal of attention in theoretical studies [7,8]. As one of the fundamental degrees of freedom in nuclei, clustering is regarded as a balance between Pauli-blocking effects and nucleon-nucleon interactions in nuclear many-body dynamics [9,10]. Numerous microscopic models have been put forward to describe the cluster states. The proposed Tohsaki-Horiuchi-Schuck-Röpke (THSR) wave function, rooted in the nonlocalized clustering concept, can well describe the dilute gaslike state of clusters [11–17]. Starting from the first principles of nuclear forces of chiral effective field theory, the no-core shell model is also a powerful approach to the study of cluster features in light nuclei [18–20]. Based on the microscopic energy density functionals (EDFs) [21], the mean-field approach could characterize single-nucleon localization and the formation of cluster structures on an equal footing [22–25].

Localization of density distributions is an essential prerequisite for the formation of cluster structures [22]. Electron scattering is considered as an effective method to investigate the nuclear density distributions, because the mechanism of electromagnetic interaction is well understood [26,27]. Over the past decades, the charge density distributions of most stable nuclei have been precisely measured by electron scattering experiments [28]. With the new radioactive isotope facilities built at RIKEN [29,30] and GSI [31,32], the structures of exotic nuclei can be studied by electron scattering in the near future.

To extract the density distributions from the experimental data of elastic electron scattering, the distorted wave Born approximation (DWBA) method has been developed by including the Coulomb distortion effects. Combining the DWBA method and nuclear structure models, the charge form factors $|F_C(q)|^2$ are systematically investigated to show the validity of the nuclear structure models [33–42]. It has been proved experimentally and theoretically that most nuclei are deformed [43–45]. Further taking into account the nuclear deformation, the $|F_C(q)|^2$ of deformed nuclei were first studied in Refs. [46,47]. With this approach, the changing trends of $|F_C(q)|^2$ of Sn and Xe isotopes were calculated in Refs. [48,49] based on the deformed mean-field calculations.

Apart from the density distributions in coordinate space, the cluster information can be reflected by the localization in momentum space. The nuclear momentum distributions can

*liujian@upc.edu.cn
†wrs16@suda.edu.cn

be extracted from the inclusive electron scattering, a process in which only the scattered electron is detected and the final nuclear state is undetermined [50–54]. With the increase of the energy transfer ω of incident electrons, the cross sections can be divided into several regions [51]. At low energy transfer, elastic scattering plays major role in this region [55]. For larger energy loss ω, termed the quasielastic (QE) region, the electrons not only interact with the total nuclei but also scatter from the individual nucleon [56]. Further increasing the electron's energy, a nucleon can be excited to form a Δ (l232) particle [57]. At very large ω, the "deep inelastic scattering" region reflects the structureless continuum on quarks bound in nucleons [58]. During the past few decades, the nuclear momentum distributions of several nuclei have been precisely obtained from the inclusive electron scattering [59–61].

The theoretical inclusive cross sections can be divided into a product of the elementary elastic cross sections and a scaling function. Studies of scaling function were first performed based on the relativistic Fermi gas (RFG) model, where the nucleus is considered as a noninteracting gas of nucleons [62]. As an extension of RFG model, the coherent density fluctuation model (CDFM) was developed for spherical nuclei by the ansatz of the generator coordinate method (GCM) and the δ-function approximation [63]. It presents the connections between the scaling functions and the nuclear structures, i.e., the density and momentum distributions [64,65]. With the CDFM approach, the inclusive electron scattering cross sections can be derived.

This paper aims to study the nuclear cluster structure of ground states by the elastic and inclusive electron scattering. The nuclei ^{12}C, ^{16}O, and ^{20}Ne are chosen as the candidates, because they usually serve as the benchmark in cluster studies. First, the EDFs are used to investigate the cluster information of ground states. It is noted that the origin of the cluster formation can be traced back to the effective nuclear interaction [66,67]. Based on a self-consistent effective nuclear interaction, the EDFs are constructed and regarded as a comprehensive approach to study the nuclear structure. By removing the degeneracy of single-nucleon levels in spherical symmetry, the deformation in effective nuclear interaction of EDFs motivates the formation of cluster structures [22]. Moreover, the DWBA and CDFM method are applied to calculate the elastic form factors and inclusive cross sections, respectively. As a precise approach, the DWBA method contains the Coulomb distortion effects, and makes it possible to provide quantitatively accurate descriptions of elastic electron scattering. The CDFM is suggested as a suitable model for studying the scaling functions of inclusive electron scattering, which allows one to investigate simultaneously the density and momentum distributions. However, because the CDFM was developed based on spherical symmetry [68,69], some moderate assumptions are made in this paper when applied to the deformed configurations of nuclei.

The theoretical studies of cluster from EDFs are associated with the calculations of electron scattering in this paper. First, based on the deformed relativistic Hartree-Bogoliubov (RHB) model, the intrinsic density distributions of normal and cluster states are calculated for the selected nuclei. Next, with the density distributions of different configurations, the corresponding elastic form factors $|F_C(q)|^2$ of selected nuclei are studied by the DWBA method, and the inclusive cross sections are calculated within the framework of CDFM. Finally, comparing the elastic form factors and inclusive cross sections of different states, the $|F_C(q)|^2$ of cluster states have definite changes in the shapes and the positions of diffraction minima. There are also noticeable variations of the inclusive cross sections of cluster states in the peak and dip regions. Therefore, the nuclear cluster structure can be revealed from the differences of cross sections of electron scattering, which can be measured in future experiments. The studies in this paper provide a new and effective method to investigate the cluster structures. It can also be used to extract the nucleon distributions in coordinate and momentum spaces from future electron scattering experiments.

This paper is organized as follows: In Sec. II, the theoretical frameworks of the deformed RHB model, DWBA, and CDFM method are provided. In Sec. III, the numerical results and discussions are presented. Finally, a summary is given in Sec. IV.

II. THEORETICAL FRAMEWORK

In this section, the theories of the relativistic Hartree-Bogoliubov (RHB) model are first provided to calculate the nuclear structure information. Besides, the frameworks of the distorted wave Born approximation (DWBA) and coherent density fluctuation model (CDFM) are presented to study the elastic and inclusive electron scattering separately.

A. Axially deformed relativistic Hartree-Bogoliubov model

The RHB model provides a unified solution of the nuclear mean-filed and paring correlations; the starting point is the effective Lagrangian density [70]

$$\begin{aligned}\mathcal{L} = {} & \bar{\psi}(i\gamma\cdot\partial - m)\psi + \frac{1}{2}(\partial\sigma)^2 - \frac{1}{2}m_\sigma\sigma^2 - \frac{1}{4}\Omega_{\mu\nu}\Omega^{\mu\nu} \\ & + \frac{1}{2}m_\omega^2\omega^2 - \frac{1}{4}\vec{R}_{\mu\nu}\vec{R}^{\mu\nu} + \frac{1}{2}m_\rho^2\vec{\rho}^2 - \frac{1}{4}F_{\mu\nu}F^{\mu\nu} - g_\sigma\bar{\psi}\sigma\psi \\ & - g_\omega\bar{\psi}\gamma\cdot\omega\psi - g_\rho\bar{\psi}\gamma\cdot\vec{\rho}\vec{\tau}\psi - e\bar{\psi}\gamma\cdot A\frac{(1-\tau_3)}{2}\psi,\end{aligned} \tag{1}$$

where the couplings of the $g_\sigma, g_\omega, g_\rho$ are the density dependence.

From the variation of Eq. (1), the Dirac equation of the single-nucleon and Klein-Gordon equations of mesons can be deduced. Pairing correlations are indispensable for a quantitative analysis of open-shell nuclei. The RHB model includes particle-hole (ph) and particle-particle (pp) correlations by the RHB equation in a mean-field approximation:

$$\begin{pmatrix} \hat{h}_D - m - \lambda & \hat{\Delta} \\ -\hat{\Delta}^* & -\hat{h}_D^* + m + \lambda \end{pmatrix}\begin{pmatrix} U_k \\ V_k \end{pmatrix} = E_k\begin{pmatrix} U_k \\ V_k \end{pmatrix}, \tag{2}$$

$\hat{h}_D$ is the Dirac Hamiltonian, and $\hat{\Delta}$ is the pairing field. U_k and V_k represent the quasiparticle Dirac spinors

$$U_k = \begin{pmatrix} f_k^{(U)} \\ ig_k^{(U)} \end{pmatrix}, \quad V_k = \begin{pmatrix} f_k^{(V)} \\ ig_k^{(V)} \end{pmatrix}. \tag{3}$$

For axially symmetric deformed shapes, Dirac spinors are expanded independently in terms of the harmonic oscillator eigenfunctions $\Phi_\alpha(\boldsymbol{r}, s)$:

$$f_i(\boldsymbol{r}, s, t) = \sum_{\alpha}^{\alpha_{\max}} f_\alpha^{(i)} \Phi_\alpha(\boldsymbol{r}, s)\chi_{t_i}(t),$$

$$g_i(\boldsymbol{r}, s, t) = \sum_{\tilde{\alpha}}^{\tilde{\alpha}_{\max}} g_{\tilde{\alpha}}^{(i)} \Phi_{\tilde{\alpha}}(\boldsymbol{r}, s)\chi_{t_i}(t). \tag{4}$$

Substituting Eqs. (3) and (4) into the Eq. (2), the coefficients $f_\alpha^{(i)}$ and $g_{\tilde{\alpha}}^{(i)}$ can be obtained. Combining the Klein-Gordon equations of mesons, the RHB equation is solved iteratively until the desired accuracy is achieved. With the Dirac spinors of nucleons, the nucleon density distributions can be calculated. Neglecting the effects from the neutron, one obtains the charge density distributions $\rho_C(\mathbf{r})$ by integrating the single-proton charge distributions

$$\rho_C(\mathbf{r}) = \int \rho_p(\mathbf{r}')\rho^p(|\mathbf{r} - \mathbf{r}'|)d\mathbf{r}', \tag{5}$$

where $\rho^p(r) = \frac{\Lambda^3}{8\pi}e^{-\Lambda r}$ with $\Lambda = 842.61$ MeV.

B. Elastic electron scattering

With the deformed density distributions obtained from RHB model, the elastic charge form factors are further investigated by the DWBA method.

The deformed charge densities $\rho_C(\mathbf{r})$ are first expanded by the Legendre function [71]

$$\begin{aligned} \rho_C(r, z) &= \sum_k \rho_k(R)P_k(\cos\theta) \\ &= \rho_0(R) + \rho_2(R)P_2(\cos\theta) + \cdots, \end{aligned} \tag{6}$$

In the framework of the plane wave Born approximation (PWBA) method, the Coulomb form factors $|F_C(q)|^2$ are expressed as the Fourier transformation of charge density distributions, and can be decomposed into several Coulomb multipoles [47],

$$|F_C(q)|^2 = \sum_{\lambda=0,2,\ldots}^{2J} |F^{C\lambda}(q)|^2, \tag{7}$$

where the Coulomb multipoles are deduced from the charge density multipoles,

$$F^{C\lambda} = 4\pi \frac{\langle Jk\lambda 0 \mid J\lambda Jk\rangle}{Z\sqrt{2\lambda+1}} \int r^2 \rho_\lambda(r) j_\lambda(qr) dr. \tag{8}$$

Combining Eqs. (7) and (8), the $|F_C(q)|^2$ can be obtained within the PWBA method. However, the nuclear Coulomb distorted effects are not included by the PWBA method. To obtain more precise results, the DWBA method is applied in this paper.

For the $C0$ multipole, the distorted wave function of the scattered electron can be given by solving the Dirac equation with spherical Coulomb potential $V_C(r)$:

$$[\boldsymbol{\alpha} \cdot \boldsymbol{p} + \beta m + V_C(r)]\Psi(\mathbf{r}) = E\Psi(\mathbf{r}). \tag{9}$$

With the direct scattering amplitude $f(\theta)$ and spin-flip scattering amplitude $g(\theta)$ calculated from Eq. (9), one obtains the $C0$ multipole in the DWBA form

$$F^{C0}(q) = (|f(\theta)|^2 + |g(\theta)|^2)/\sigma_{\text{Mott}}, \tag{10}$$

where σ_{Mott} is the Mott scattering cross section.

Higher multipoles $F^{C\lambda}$, which are much smaller than F^{C0} and only affect the diffraction minima of $|F_C(q)|^2$, are investigated by the PWBA method. With Eqs. (6) and (7)–(10) we can finally obtain the DWBA form factors.

C. Inclusive electron scattering

In the electron energy range of ≈ 1 GeV, there are two dominant dynamical mechanisms: quasielastic (QE) scattering and Δ resonance.

1. Coherent density fluctuation model

Studies of scaling functions are first performed on the basis of the relativistic Fermi gas (RFG) model. But it is unable to reflect the detailed nuclear structure. CDFM is further proposed to study the scaling functions, where the nuclear structure information is included.

The scaling function $f^{\text{QE}}(\psi')$ in CDFM can be written as an asymmetrical form [72]:

$$f^{\text{QE}}(\psi') = f_1^{\text{QE}}(\psi') + f_2^{\text{QE}}(\psi'), \tag{11}$$

where the asymmetry scaling functions can be written as

$$\begin{aligned} f_1^{\text{QE}}(\psi') &\cong \int_0^{\alpha/k_F|\psi'|} dR|F(R)|^2 \mathscr{F}_1(R, \psi'), \quad \psi' \leqslant 0, \\ f_2^{\text{QE}}(\psi') &\cong \int_0^{c_2\alpha/k_F|\psi'|} dR|F(R)|^2 \mathscr{F}_2(R, \psi'), \quad \psi' \geqslant 0, \end{aligned} \tag{12}$$

with

$$\begin{aligned} \mathscr{F}_1(R, \psi') &= c_1 \times \left[1 - \left(\frac{k_F R|\psi'|}{\alpha}\right)^2\right], \\ \mathscr{F}_2(R, \psi') &= c_1 \times \left[1 - \left(\frac{k_F R|\psi'|}{c_2\alpha}\right)^2\right]. \end{aligned} \tag{13}$$

The weight function $|F(R)|^2$ is strongly linked to the nuclear density distributions

$$|F(R)|^2 = -\frac{1}{\rho_0(R)} \frac{d\rho(r)}{dr}\bigg|_{r=R}, \quad \rho_0(R) = \frac{3A}{4\pi R^3}, \tag{14}$$

and $\alpha = (\frac{9\pi A}{8})^{1/3}$.

In the QE region, the scaling variable ψ' is defined as [73]

$$\psi' \equiv \frac{1}{\sqrt{\xi_F}} \frac{\lambda' - \tau'}{\sqrt{(1+\lambda')\tau' + \kappa\sqrt{\tau'(\tau'+1)}}}. \tag{15}$$

The k_F is Fermi momentum. In CDFM, the coefficients are given by modifying the nuclear structure model and the

phenomenological fit of the experimental data, where $c_1 = 0.72$ and $c_2 = 13/12$.

Substituting Eq. (14) into Eq. (12), we can obtain the following expression:

$$f_i^{\mathrm{QE}}(\psi') = \frac{4\pi}{A}\int_0^{\mathscr{R}_i} dR\,\rho(R)\left[R^2\mathscr{F}_i(R,\psi') + \frac{R^3}{3}\frac{\partial\mathscr{F}_i(R,\psi')}{\partial R}\right], \tag{16}$$

where $i = 1$ for $\psi' \geqslant 0$, and $i = 2$ for $\psi' \leqslant 0$. The density distribution $\rho(R)$ in Eq. (16) is spherical, and the CDFM is developed for the spherical nuclei. For example, in Refs. [68,69], the authors investigated the magnetic form factors of odd-A nuclei based on the deformed mean-field method where the CDFM is applied only to the spherical nuclei. In order to study the scaling properties of deformed configurations, in this paper, a moderate approximation is made when applying the scaling function of CDFM model. Instead of the density $\rho(R)$ of spherical nucleus, we use the spherical part $\rho_0(R)$ of the deformed densities in Eq. (6) to calculate the scaling function of Eq. (16). This is acceptable because the spherical part $\rho_0(R)$ is the major component of the deformed distribution. Besides, if we use the deformed density $\rho(R,\theta)$ of Eq. (6) instead of $\rho(R)$ and integrate over the angular θ of intrinsic coordinate system, the contributions of the deformed components disappear automatically and only the spherical component is left.

In this paper, the analysis is extended to the Δ-resonance region. The scaling variable in the Δ region is introduced by Ref. [74]:

$$\psi'_\Delta \equiv \left[\frac{1}{\xi_F}\left(\kappa\sqrt{\rho'^2_\Delta + 1/\tau'} - \lambda'\rho'_\Delta - 1\right)\right]^{1/2} \times \begin{cases} +1, & \lambda' \geqslant \lambda'^0_\Delta, \\ -1, & \lambda' \leqslant \lambda'^0_\Delta. \end{cases} \tag{17}$$

The Δ-scaling function $f^\Delta(\psi'_\Delta)$ in the CDFM is defined as

$$f^\Delta(\psi'_\Delta) = \int_0^\infty dR|F(R)|^2 f^\Delta_{\mathrm{RFG}}[\psi'_\Delta(R)], \tag{18}$$

where the RFG superscaling function in the Δ domain is

$$f^\Delta_{\mathrm{RFG}}(\psi'_\Delta) = \tfrac{3}{4}\left(1-\psi'^2_\Delta\right)\Theta\left(1-\psi'^2_\Delta\right). \tag{19}$$

In CDFM calculations, the value 3/4 is replaced by 0.54 based on the nuclear structure studies.

2. Cross sections in the quasielastic region

In the one-photon-exchange approximation, the double differential cross sections of inclusive electron scattering can be written as the functions of momentum transfer q and energy transfer ω:

$$\frac{d^2\sigma}{d\Omega_{k'}d\epsilon'} = \sigma_M\left[\left(\frac{Q^2}{q^2}\right)^2 R_L(q,\omega) + \left(\frac{1}{2}\left|\frac{Q^2}{q^2}\right| + \tan^2\frac{\theta}{2}\right)R_T(q,\omega)\right]. \tag{20}$$

R_L and R_T are the longitudinal and transverse response functions, respectively. They contain the information of nuclear electromagnetic charge and current density distribution.

In the QE region, $R_{L(T)}$ can be expressed by the scaling functions in Eq. (11) [74]:

$$R_L^{\mathrm{QE}}(\kappa,\lambda) = \Lambda_0\frac{\kappa^2}{\tau}[(1+\tau)W_2(\tau) - W_1(\tau)] \times f^{\mathrm{QE}}(\psi'),$$
$$R_T^{\mathrm{QE}}(\kappa,\lambda) = \Lambda_0[2W_1(\tau)] \times f^{\mathrm{QE}}(\psi'), \tag{21}$$

where $W_1(\tau)$, $W_2(\tau)$ are linked to the Sachs form factors $G_E(\tau)$, $G_M(\tau)$. Substituting Eq. (21) into Eq. (20), the quasielastic electron scattering cross sections can be obtained.

3. Cross sections in the Δ resonance region

As the ω increases, the Δ resonance becomes the main effect in inclusive electron scattering. With the scaling function Eq. (18), the longitudinal and transverse response functions $R_{L(T)}$ in this region are calculated as [75]

$$R_L^\Delta(\kappa,\lambda) = \frac{\mathcal{N}\xi_F}{2m_N\eta_F^3\kappa}\frac{\kappa^2}{\tau}[(1+\tau\rho^2)w_2(\tau) - w_1(\tau) + w_2(\tau)D(\kappa,\lambda)] \times f^\Delta(\psi'_\Delta),$$
$$R_T^\Delta(\kappa,\lambda) = \frac{\mathcal{N}\xi_F}{2m_N\eta_F^3\kappa}[2w_1(\tau) + w_2(\tau)D(\kappa,\lambda)] \times f^\Delta(\psi'_\Delta), \tag{22}$$

where $\mathcal{N} = N, Z$.

Substituting Eq. (22) into Eq. (20), the Δ resonance cross sections are calculated. Combining the contributions of QE and Δ regions, the total cross sections of inclusive electron scattering can be obtained.

III. NUMERICAL RESULTS AND DISCUSSIONS

As mentioned in the Introduction, the cluster formation plays significant role in investigating the structure of light nuclei and coexists with the nuclear mean field. In this section, cluster structures of selected nuclei (^{12}C, ^{16}O, and ^{20}Ne) are investigated with the self-consistent relativistic Hartree-Bogoliubov (RHB) model with the DD-ME2 parameter set. The corresponding Coulomb form factors and inclusive electron scattering cross sections are also calculated with the formulas of Sec. II.

A. ^{12}C

The binding energies of ^{12}C from the constrained calculations of the RHB model with DD-ME2 functional are presented as a function of deformation parameter β_2 in Fig. 1. There are three minima, located at $\beta_2 = -0.33$, 0.03, and 2.36. From this figure, one can see that the ground state of ^{12}C has an oblate shape for $\beta_2 = -0.33$ and the binging energy agrees with the experimental data $B_{\mathrm{exp}} = 92.2$ MeV. We also provide the corresponding intrinsic nucleon density distributions in the insets of Fig. 1. It is noted that, removing the degeneracy of single-nucleon levels related to spherical symmetry, deformation plays a significant role in the formation of clusters. In our calculation, the 3α-chain configuration shows up for the deformation $\beta_2 = 2.36$. This indicates higher deformation is favorable for the formation of clusters in light nuclei. The reason is that the deformation increases the nuclear

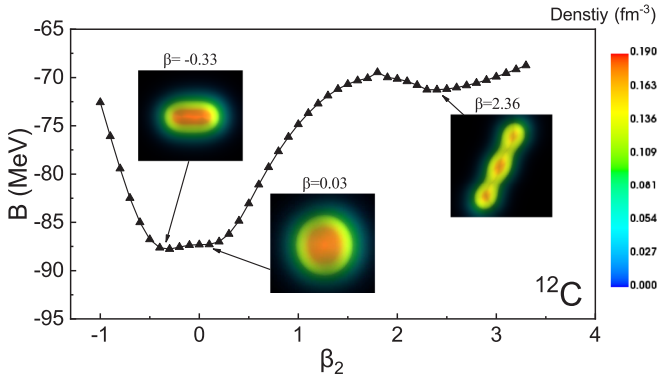

FIG. 1. Binding energies of ^{12}C as a function of the deformation parameter β_2 from the constrained RHB calculations with DD-ME2 functional. The insets display the corresponding nucleon density distributions.

potential depth and makes the wave functions more localized. The RHB model can provide reasonable descriptions for the study of nuclear properties, which is also confirmed in many researches [70,76]. By the constrained RHB model, in this paper the formation of α clusters is shown without presupposing the existence of cluster structures.

The Coulomb form factors $|F_C(q)|^2$ can reflect nuclear electromagnetic structures precisely. To further analyze the intrinsic density distributions in Fig. 1, the corresponding $|F_C(q)|^2$ of ^{12}C are calculated by the DWBA method, and the results are presented in Fig. 2. One can see that the experimental form factors can be reproduced by the DWBA calculations. In Fig. 2, the $|F_C(q)|^2$ of ^{12}C for $\beta_2 = -0.33$ and $\beta_2 = 0.03$ are similar, because their charge root-mean-square radii (R_C) are relatively close to each other. However, owing to the effects of nuclear deformation, the diffraction minimum of $|F_C(q)|^2$ of $\beta_2 = -0.33$ has a downward and outward shift, compared with that of $\beta_2 = 0.03$. As the deformation further

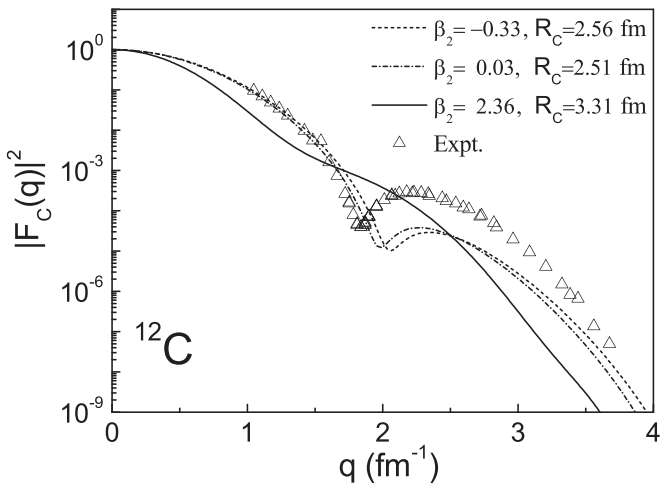

FIG. 2. $|F_C(q)|^2$ of ^{12}C for deformation parameter $\beta_2 = -0.33$, 0.03, and 2.36, calculated by the DWBA method. The corresponding $\rho_C(r)$ are from the constrained RHB calculations. The experimental data are taken from Ref. [77].

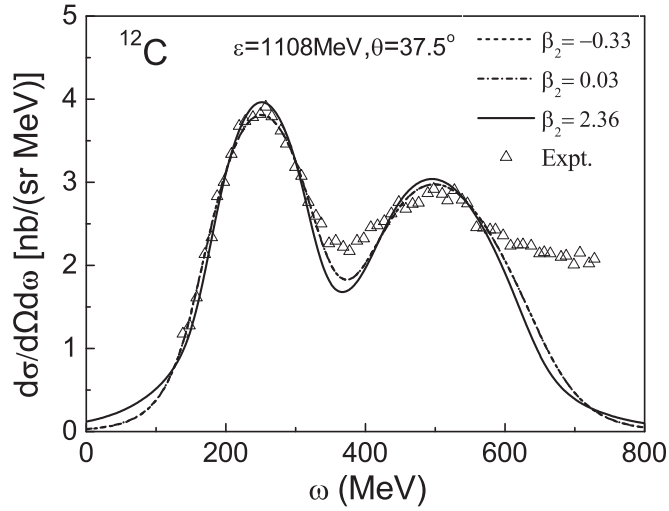

FIG. 3. Inclusive electron scattering cross sections of ^{12}C for different deformations at incident energy $\varepsilon = 1108$ MeV and $\theta = 37.5°$. The results are calculated by CDFM, where the density distributions are from constrained RHB calculations. The experimental data are taken from Ref. [80].

increases, the 3α-cluster structure tends to be formed, which has essential influence on the corresponding $|F_C(q)|^2$ of Fig. 2. For this state, there are more pronounced changes in the shape of $|F_C(q)|^2$, and the diffraction minimum at $q \approx 1.5$ fm^{-1} becomes flat. Therefore, the $|F_C(q)|^2$ can reflect the influences of the cluster on the density distributions. The discrepancies of $|F_C(q)|^2$ mean the cluster structure of the ground state of ^{12}C can be detected by the elastic electron scattering.

Elastic scattering makes it possible to measure the density distributions in coordinate space, and the inclusive quasielastic electron scattering provides the information of nucleon momentum distributions. To further illustrate the differences between the cluster and normal state in momentum space, we provide the total inclusive cross sections of ^{12}C with the CDFM in Fig. 3, where the corresponding density distributions are from Fig. 1. Because the CDFM can only be applied under spherical symmetry [68,69], in this part the spherical components $\rho_0(r)$ instead of the total density distributions $\rho(\mathbf{r})$ are used in the framework of CDFM. For $\beta_2 = -0.33$ and $\beta_2 = 0.03$, there are similar results of cross sections in Fig. 3, because their deformation parameters are close to each other. Both of them give reasonable descriptions of the experimental data, which also examines the validity and suitability of CDFM. For the biggest deformation $\beta_2 = 2.36$ with the 3α-cluster structure, the regions of the peak and dip have distinct discrepancies. The differences of cross sections in Fig. 3 represent the discrepancies of momentum distributions, and are also highly connected with the density distributions in coordinate space. Because the density distributions can be turned into momentum distributions by the Fourier transform of nucleon wave functions, the cross sections in Fig. 3 can reflect the cluster structure in Fig. 1. Comparing the theoretical results with the experimental data of electron scattering in Figs. 2 and 3, we can draw the conclusion that the ground

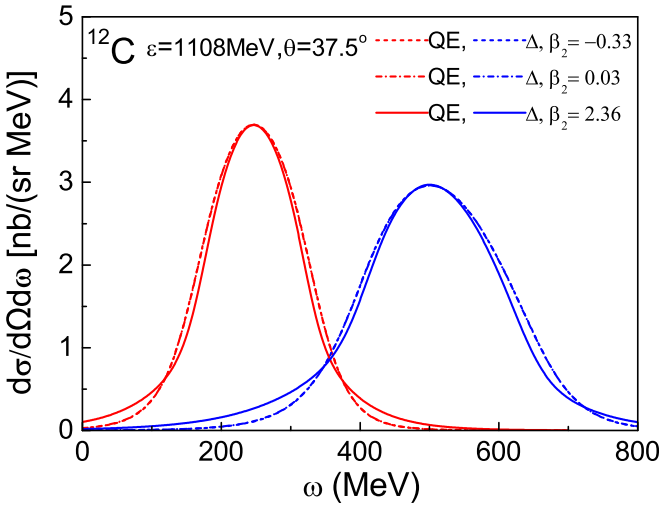

FIG. 4. The contributions on inclusive cross sections of Fig. 3 from QE and Δ regions, respectively.

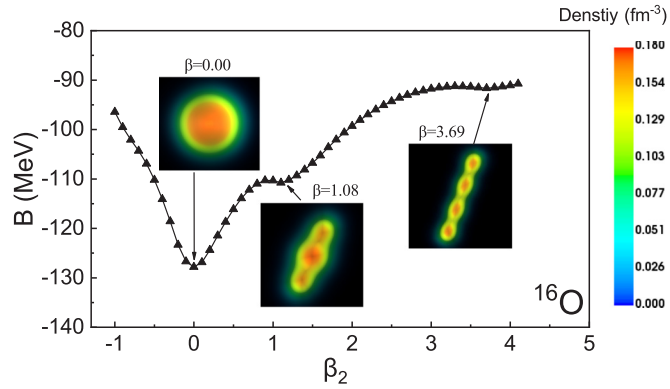

FIG. 5. Binding energies of ^{16}O as a function of the deformation parameter β_2 from the constrained RHB calculations with the DD-ME2 functional. The insets display the corresponding nucleon density distributions.

state of ^{12}C mainly shows the mean-field structure rather than the cluster structure.

To better explain the discrepancies of different states in Fig. 3, we further present the contributions from the QE and Δ regions to inclusive cross sections separately in Fig. 4. As can be shown, the positions of QE and Δ peaks are identical for different deformation parameters. Because of the energy and momentum conservation, the inclusive cross sections have a peak located at $\omega = q^2/2M$, which corresponds to the energy taken from the recoiling nucleons with $p = 0$ [78]. The width of the peak is another important characteristic in the study of inclusive electron scattering, and is directly proportional to the Fermi momentum k_F [54]. It is noted that k_F is inversely correlated with the nuclear radii R [79]. The cluster state $\beta_2 = 2.36$ has the biggest R and the smallest k_F, so the width of the peak is the narrowest both in QE and Δ regions. The total cross sections of Fig. 3 are the superposition of QE and Δ contributions. For this reason, the 3α-cluster state has the biggest value of the QE and Δ peaks and the smallest value of dip. Combining Figs. 3 and 4, one can draw a conclusion that inclusive electron scattering can be used to analyze the cluster structure.

B. ^{16}O

Besides ^{12}C, ^{16}O is also chosen to investigate the cluster structure. The binding energies of ^{16}O are presented in Fig. 5. As can be seen, there are three minima, located at $\beta_2 = 0.0$, 1.08, and 3.69, which represent the different nuclear configurations. In the insets of Fig. 5, the corresponding intrinsic nucleon density distributions are included. Being a doubly magic nucleus, it has a spherical shape for ^{16}O at the state $\beta_2 = 0.0$. The theoretical binding energy of this state can well reproduce the experimental result $B_{\rm exp} = 127.6$ MeV, which verifies the reliability of the RHB model to describe the nuclear ground properties. Considering the role of deformation, the density distributions are inhomogeneous and the shape of ^{16}O becomes axial prolate for $\beta_2 = 1.08$. For the biggest deformation $\beta_2 = 3.69$, the linear 4α-chain structure is well depicted in Fig. 5. It further proves that the formation of clusters is favored at higher deformation.

In Fig. 5, we provide the ground state densities for different deformations. The corresponding Coulomb form factors $|F_C(q)|^2$ and charge radii R_C are calculated and presented in Fig. 6. It can be seen that the theoretical $|F_C(q)|^2$ of $\beta_2 = 0.00$ are consistent with the experimental data, because ^{16}O is a typical spherical nucleus. For $\beta_2 = 1.08$, the deformation has an essential influence on $|F_C(q)|^2$, where the positions of diffraction minima have an obvious downward and outward shift. Further increasing the deformation, the intrinsic density distributions become more localized and the 4α-cluster configuration shows up at the state of $\beta_2 = 3.69$. The $|F_C(q)|^2$ of this state have no obvious diffraction minimum at $q \approx 1.0$ fm^{-1} and the shape also changes a lot. These behaviors

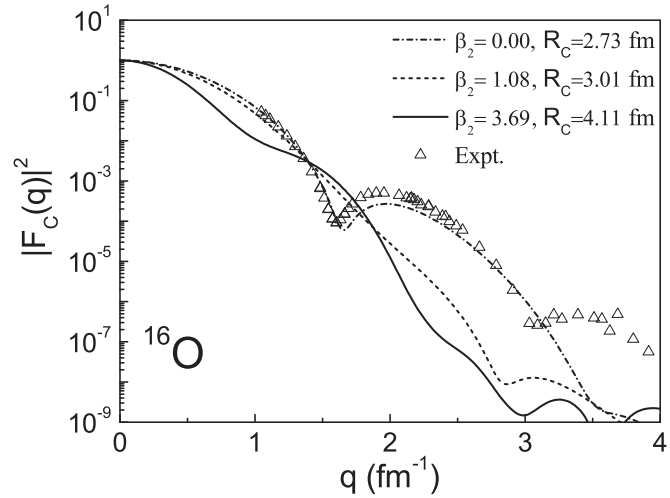

FIG. 6. $|F_C(q)|^2$ of ^{16}O for deformation parameter $\beta_2 = 0.0$, 1.08, and 3.69, calculated by the DWBA method. The corresponding $\rho_C(r)$ are from the constrained RHB calculations. The experimental data are taken from the Ref. [77].

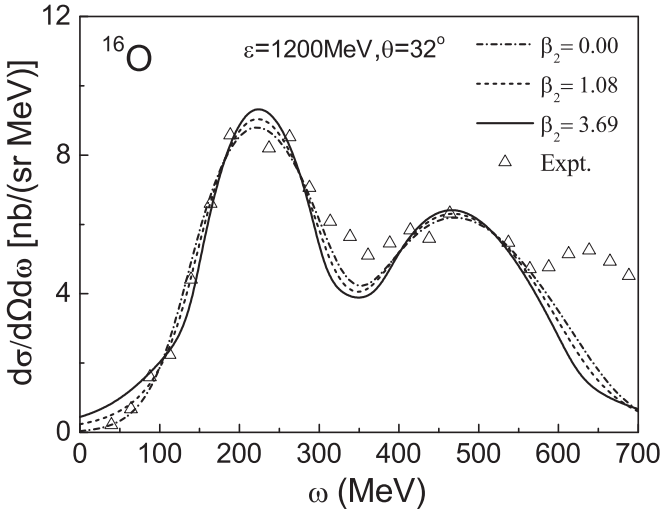

FIG. 7. Inclusive electron scattering cross sections of ^{16}O for different deformations at incident energy $\varepsilon = 1200$ MeV and $\theta = 32°$. The results are calculated by CDFM, where the density distributions are from constrained RHB calculations. The experimental data are taken from Ref. [81].

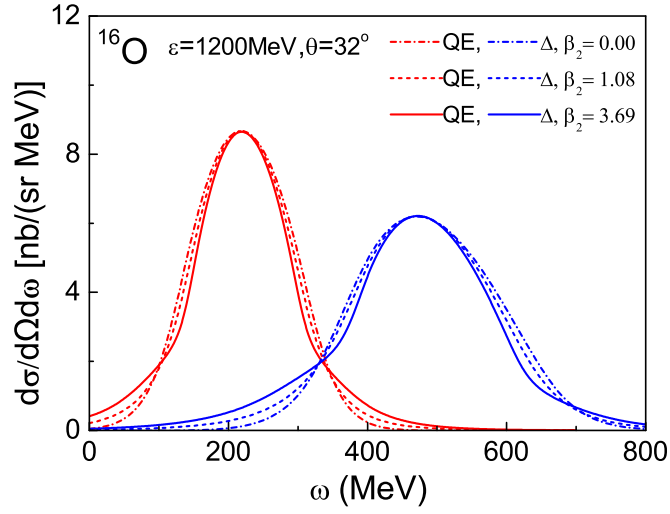

FIG. 8. The contributions on inclusive cross sections of Fig. 7 from QE and Δ regions.

show the effects of the cluster structure on$|F_C(q)|^2$, which are similar to those in Fig. 2 of ^{12}C.

To show the influences of the cluster state in nucleon momentum distributions, the total inclusive cross sections of ^{16}O for different states are presented in Fig. 7 using the CDFM. During the calculations, we also use the spherical parts $\rho_0(r)$ of densities instead of the deformed distribution $\rho(\mathbf{r})$ as an approximation in Eq. (16). As can be seen in this figure, the results of $\beta_2 = 0.00$ coincide better with the experimental data. For the configuration $\beta_2 = 3.69$ with the 4-α cluster structure, its QE peak and dip have distinct changes with those of $\beta_2 = 1.08$ and $\beta_2 = 0.00$. From the comparisons of the Coulomb form factors and inclusive cross sections in Figs. 6 and 7, similar results show that the ground state of ^{16}O is the mean-field state instead of the cluster structure. With the purpose of illustrating the differences in Fig. 7 between the normal and cluster state, the contributions of QE and Δ regions to inclusive cross sections are presented in Fig. 8. In this figure, the positions of QE and Δ peaks for different deformations are the same. With the increase of the deformation, the nuclear radii in r-space become larger but the Fermi momenta k_F in p-space become smaller. Due to the width of the peak is in direct proportion to the k_F, the state with the 4-α configuration has the narrowest peak for QE and Δ regions in Fig. 8. The differences in the widths of the QE and Δ peaks cause the differences in the cross sections of Fig. 7. Therefore, the distinctions in inclusive cross sections between different states can reflect the effects of the 4-α cluster structure.

C. ^{20}Ne

Apart from ^{12}C and ^{16}O, the binding energies of ^{20}Ne are also given in Fig. 9. The minima of the curve locate at $\beta_2 = -0.16$, 0.55, and 2.14, which correspond to the different shapes of nuclei. In Fig. 9, we provide the intrinsic nucleon density distributions accordingly in the insets. It can be seen that the ground state of ^{20}Ne exhibits an oblate shape for $\beta_2 = -0.16$. Increasing the deformation, the equilibrium shape becomes prolate for $\beta_2 = 0.55$, and the theoretical binding energy of this state agrees with the experimental data $B_{\text{exp}} = 160.6$ MeV. There are two pronounced nucleon localizations with a deformed oblate core for this state, which displays an α-^{12}C-α structure. Similar results are obtained in Ref. [24]. As mentioned above, the deformation can enhance the formation of α clusters. For the configuration $\beta_2 = 2.14$, the intrinsic density distribution displays a linear chain structure.

With the density distributions of different deformations in Fig. 9, the corresponding Coulomb form factors $|F_C(q)|^2$ and charge radii R_C are investigated and presented in Fig. 10. As shown in this figure, for the mean-field structure $\beta_2 = -0.16$ and α-^{12}C-α structure $\beta_2 = 0.55$, the R_C are close to each other, and the $|F_C(q)|^2$ of the two states are also similar. Both of them are in accordance with the elastic scattering

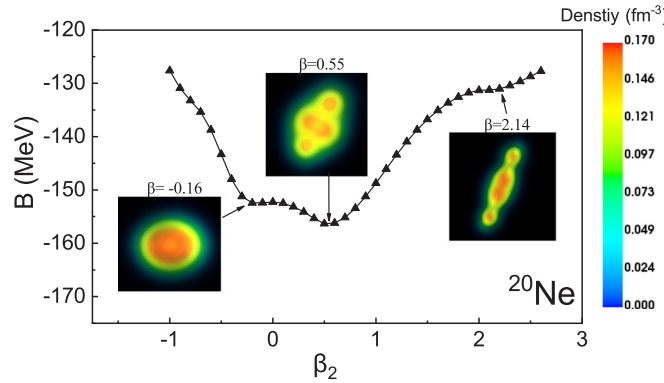

FIG. 9. Binding energies of ^{20}Ne as a function of the deformation parameter β_2 from the constrained RHB calculations with DD-ME2 functional. The insets display the corresponding nucleon density distributions.

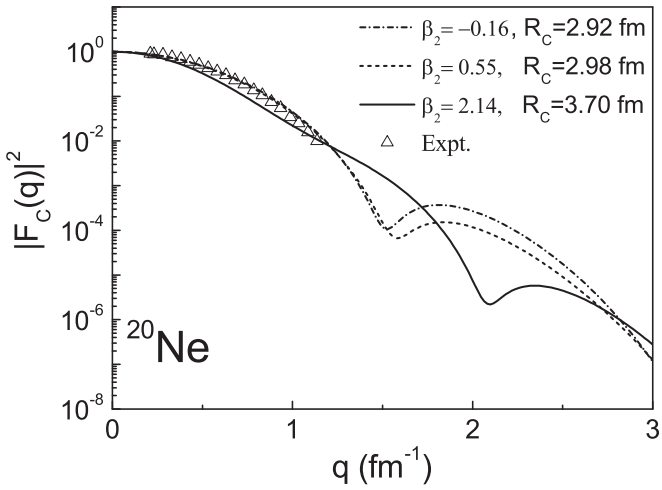

FIG. 10. $|F_C(q)|^2$ of ^{20}Ne for deformation parameter $\beta_2 = -0.16$, 0.55, and 2.14, calculated by the DWBA method. The corresponding $\rho_C(r)$ are from the constrained RHB calculations. The experimental data are taken from the Ref. [82].

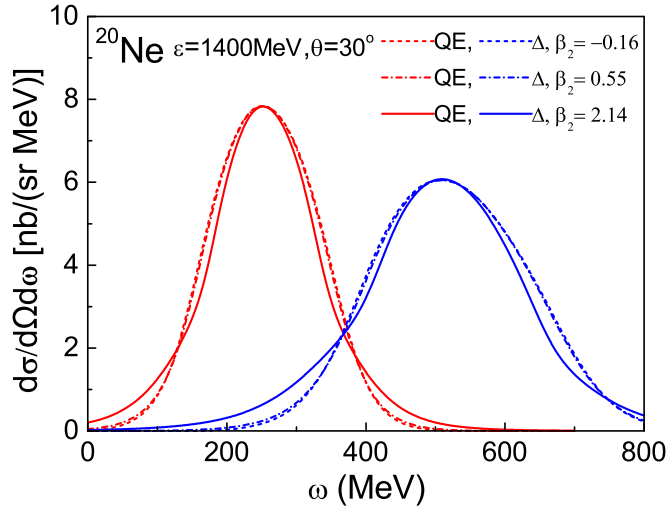

FIG. 12. The contributions on inclusive cross sections of Fig. 11 from QE and Δ regions, respectively.

experimental data. For the linear chain state $\beta_2 = 2.14$, the diffraction minimum of the $|F_C(q)|^2$ has a noticeable shift toward high momentum transfer q and the values of the minimum decrease. The $|F_C(q)|^2$ reflect the effects of the cluster structure on density distributions, therefore, the linear chain structure causes the variations in $|F_C(q)|^2$ of ^{20}Ne. From Fig. 10, one can see that the linear chain structure is ruled out for the ground state of ^{20}Ne, and further experimental measurements are needed at the region $q \approx 1.5$ fm^{-1} to distinguish the mean-field state and α-^{12}C-α state.

To better study the density distributions of different states of Fig. 9 in momentum space, the corresponding inclusive cross sections are calculated and provided in Fig. 11. It is shown that the cross sections of $\beta_2 = -0.16$ and $\beta_2 = 0.55$ are close to each other in general. The linear chain state $\beta_2 = 2.14$ has differences in the peak and dip regions. If the inclusive cross sections are measured for ^{20}Ne, it will be helpful to study the mean-field structure and the cluster structure at the ground state. In Fig. 12, we also present the contributions on inclusive cross sections from QE and Δ regions separately to interpret this phenomenon. As can be seen, the width of the peak of the linear chain state is the narrowest in both QE and Δ regions, which is due to the smallest k_F of this state. The discrepancies in the width of the peak in Fig. 12 give rise to the differences in the corresponding cross sections of Fig. 11. These variations of inclusive cross sections between cluster and normal states are similar to those of ^{12}C and ^{16}O in Figs. 3 and 7. Therefore, the inclusive electron scattering also provides a suitable method to detect the cluster structure.

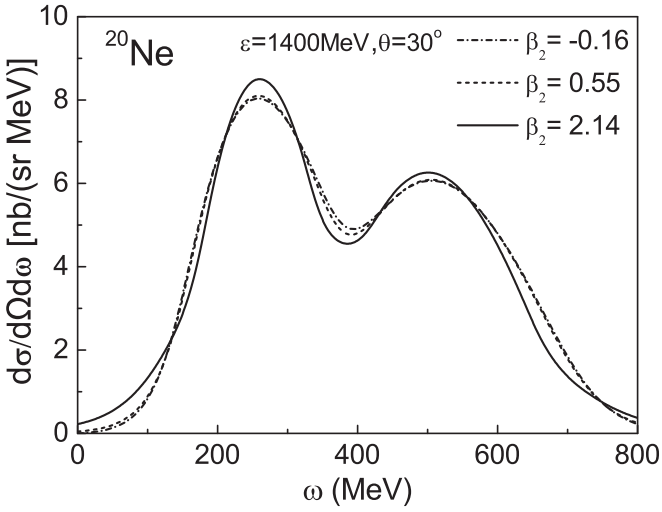

FIG. 11. Inclusive electron scattering cross sections of ^{20}Ne for different deformations at incident energy $\varepsilon = 1400$ MeV and $\theta = 30^\circ$. The results are calculated by CDFM, where the density distributions are from constrained RHB calculations.

IV. SUMMARY

The cluster phenomenon is one of the most fundamental features in light nuclei. In this paper, we combine the nuclear structure model with the electron scattering process to study the cluster structure. During the research, the density distributions are obtained from the RHB model, and the corresponding elastic and inclusive electron scattering cross sections are calculated by the DWBA and CDFM method, respectively.

With the RHB model, the energy surfaces of selected nuclei (^{12}C, ^{16}O, and ^{20}Ne) are investigated. There are three minima for the curves, which represent the different nuclear configurations in ground states. The corresponding intrinsic density distributions of different minima are also given. It can be seen that pronounced nucleon localization exhibits at specific deformation. This is because the deformation increases the nuclear potential depth and makes the nucleon wave functions more localized, which favors the formation of cluster structures.

Combining the RHB model and DWBA method, the Coulomb form factors $|F_C(q)|^2$ of different states are calculated and compared with each other for the selected nuclei. As can be seen, the theoretical $|F_C(q)|^2$ of the normal state coincide with the experimental data well. With the increase of the localization of density distributions, the $|F_C(q)|^2$ have definite changes in the shapes and the positions of diffraction minima. The $|F_C(q)|^2$ reflect the density distributions directly; therefore, the variations of $|F_C(q)|^2$ mean the cluster structure in coordinate space can be analyzed by the elastic electron scattering.

Differing from the elastic electron scattering, the inclusive electron scattering makes it possible to measure the nucleon density distributions in momentum space. Based on the CDFM, the inclusive cross sections of the normal and cluster states of ^{12}C, ^{16}O, and ^{20}Ne are investigated and compared with each other. An approximation is made in this paper in which the spherical components $\rho_0(R)$ of the deformed configurations are used to study the scaling properties of the CDFM. For the normal states, the theoretical cross sections agree with the experimental data well. For the cluster states, there are noticeable changes of cross sections in the peak and dip regions. This can be attributed to the variations of k_F, which result in the discrepancies of the inclusive cross sections for the normal and cluster states. These results further illustrate that cluster structures can be detected by the inclusive electron scattering.

By the comparison of the theoretical form factors and inclusive cross sections with the experimental data, we find that the ground states of ^{12}C and ^{16}O present the mean-field structure. For ^{20}Ne, the linear chain state is ruled out, and further experimental measurements are needed to distinguish the mean-field structure and α-^{12}C-α structure. It should also be mentioned that the calculations of deformed configurations within the framework CDFM are only an approximate studies. An alternative scaling function and a new CDFM model are expected, if applicable, for deformed nuclei. By combining the nuclear structure model with the electron scattering theory, the method proposed in this paper provides a new and effective approach to investigate cluster configurations, and can serve as a useful guide for future electron scattering experiments.

ACKNOWLEDGMENTS

This work was supported by the National Natural Science Foundation of China (Grants No. 11505292, No. 11822503, No. 11975167, and No. 12035011), by the Shandong Provincial Natural Science Foundation, China (Grant No. ZR2020MA096), by the Fundamental Research Funds for the Central Universities (Grants No. 20CX05013A and No. 22120210138), and by the Graduate Innovative Research Funds of China University of Petroleum (East China) (Grant No. YCX2020104).

[1] M. Itoh, H. Akimune, M. Fujiwara, U. Garg, N. Hashimoto, T. Kawabata, K. Kawase, S. Kishi, T. Murakami, K. Nakanishi, Y. Nakatsugawa, B. K. Nayak, S. Okumura, H. Sakaguchi, H. Takeda, S. Terashima, M. Uchida, Y. Yasuda, M. Yosoi, and J. Zenihiro, Phys. Rev. C **84**, 054308 (2011).

[2] C. Beck, *Clusters in Nuclei*, Lecture Notes in Physics, Vol. 2 (Springer, Berlin, 2012).

[3] M. Freer, J. D. Malcolm, N. L. Achouri, N. I. Ashwood, D. W. Bardayan, S. M. Brown, W. N. Catford, K. A. Chipps, J. Cizewski, N. Curtis, K. L. Jones, T. Munoz-Britton, S. D. Pain, N. Soić, C. Wheldon, G. L. Wilson, and V. A. Ziman, Phys. Rev. C **90**, 054324 (2014).

[4] M. Freer and H. O. U. Fynbo, Prog. Part. Nucl. Phys. **78**, 1 (2014).

[5] D. J. Marín-Lámbarri, R. Bijker, M. Freer, M. Gai, T. Kokalova, D. J. Parker, and C. Wheldon, Phys. Rev. Lett. **113**, 012502 (2014).

[6] Z. H. Yang, Y. L. Ye, Z. H. Li, J. L. Lou, J. S. Wang, D. X. Jiang, Y. C. Ge, Q. T. Li, H. Hua, X. Q. Li, F. R. Xu, J. C. Pei, R. Qiao, H. B. You, H. Wang, Z. Y. Tian, K. A. Li, Y. L. Sun, H. N. Liu, J. Chen *et al.*, and Phys. Rev. Lett. **112**, 162501 (2014).

[7] W. von Oertzen, M. Freer, and Y. Kanada-En'yo, Phys. Rep. **432**, 43 (2006).

[8] M. Freer, H. Horiuchi, Y. Kanada-En'yo, D. Lee, and Ulf-G. Meißner, Rev. Mod. Phys. **90**, 035004 (2018).

[9] H. Horiuchi, K. Ikeda, and K. Katō, Prog. Theor. Phys. Suppl. **192**, 1 (2012).

[10] C. Xu, G. Röpke, P. Schuck, Z. Ren, Y. Funaki, H. Horiuchi, A. Tohsaki, T. Yamada, and B. Zhou, Phys. Rev. C **95**, 061306(R) (2017).

[11] A. Tohsaki, H. Horiuchi, P. Schuck, and G. Röpke, Phys. Rev. Lett. **87**, 192501 (2001).

[12] Y. Funaki, H. Horiuchi, W. von Oertzen, G. Röpke, P. Schuck, A. Tohsaki, and T. Yamada, Phys. Rev. C **80**, 064326 (2009).

[13] B. Zhou, Y. Funaki, H. Horiuchi, Z. Ren, G. Röpke, P. Schuck, A. Tohsaki, C. Xu, and T. Yamada, Phys. Rev. Lett. **110**, 262501 (2013).

[14] M. Lyu, Z. Ren, B. Zhou, Y. Funaki, H. Horiuchi, G. Röpke, P. Schuck, A. Tohsaki, C. Xu, and T. Yamada, Phys. Rev. C **91**, 014313 (2015).

[15] M. Lyu, Z. Ren, B. Zhou, Y. Funaki, H. Horiuchi, G. Röpke, P. Schuck, A. Tohsaki, C. Xu, and T. Yamada, Phys. Rev. C **93**, 054308 (2016).

[16] D. Bai and Z. Ren, Phys. Rev. C **101**, 034311 (2020).

[17] D. Bai and Z. Ren, Phys. Rev. C **103**, 044316 (2021).

[18] E. K. Warburton and B. A. Brown, Phys. Rev. C **46**, 923 (1992).

[19] P. Navrátil, J. P. Vary, and B. R. Barrett, Phys. Rev. Lett. **84**, 5728 (2000).

[20] A. C. Dreyfuss, K. D. Launey, T. Dytrych, J. P. Draayer, and C. Bahri, Phys. Lett. B **727**, 511 (2013).

[21] T. Nikšić, D. Vretenar, and P. Ring, Prog. Part. Nucl. Phys. **66**, 519 (2011).

[22] J.-P. Ebran, E. Khan, T. Nikšić, and D. Vretenar, Nature (London) **487**, 341 (2012).

[23] J.-P. Ebran, E. Khan, T. Nikšić, and D. Vretenar, Phys. Rev. C **87**, 044307 (2013).

[24] J.-P. Ebran, E. Khan, T. Nikšić, and D. Vretenar, Phys. Rev. C **89**, 031303(R) (2014).

[25] P. Marević, J.-P. Ebran, E. Khan, T. Nikšić, and D. Vretenar, Phys. Rev. C **99**, 034317 (2019).

[26] J. Liu, Z. Ren, and T. Dong, Nucl. Phys. A **900**, 1 (2013).
[27] J. Liu, Z. Ren, C. Xu, and R. Xu, Phys. Rev. C **88**, 054321 (2013).
[28] H. De Vries, C. W. De Jager, and C. De Vries, At. Data Nucl. Data Tables **36**, 495 (1987).
[29] T. Suda, M. Wakasugi, T. Emoto, K. Ishii, S. Ito, K. Kurita, A. Kuwajima, A. Noda, T. Shirai, T. Tamae, H. Tongu, S. Wang, and Y. Yano, Phys. Rev. Lett. **102**, 102501 (2009).
[30] K. Tsukada, A. Enokizono, T. Ohnishi, K. Adachi, T. Fujita, M. Hara, M. Hori, T. Hori, S. Ichikawa, K. Kurita, K. Matsuda, T. Suda, T. Tamae, M. Togasaki, M. Wakasugi, M. Watanabe, and K. Yamada, Phys. Rev. Lett. **118**, 262501 (2017).
[31] H. Simon, Nucl. Phys. A **787**, 102 (2007).
[32] A. N. Antonov *et al.*, Nucl. Instrum. Methods Phys. Res., Sect. A **637**, 60 (2011).
[33] A. N. Antonov, D. N. Kadrev, M. K. Gaidarov, E. Moya de Guerra, P. Sarriguren, J. M. Udias, V. K. Lukyanov, E. V. Zemlyanaya, and G. Z. Krumova, Phys. Rev. C **72**, 044307 (2005).
[34] X. Roca-Maza, M. Centelles, F. Salvat, and X. Viñas, Phys. Rev. C **87**, 014304 (2013).
[35] A. Meucci, M. Vorabbi, C. Giusti, F. D. Pacati, and P. Finelli, Phys. Rev. C **89**, 034604 (2014).
[36] J. M. Yao, M. Bender, and P.-H. Heenen, Phys. Rev. C **91**, 024301 (2015).
[37] D. H. Jakubassa-Amundsen, J. Phys. G **41**, 075103 (2014).
[38] J. Liu, C. Xu, and Z. Ren, Phys. Rev. C **95**, 044318 (2017).
[39] J. Liu, R. Xu, J. Zhang, C. Xu, and Z. Ren, J. Phys. G **46**, 055105 (2019).
[40] Y. Yang and Q. Li, J. Phys. G **47**, 035104 (2020).
[41] Y. Ma, C. Su, J. Liu, Z. Ren, C. Xu, and Y. Gao, Phys. Rev. C **101**, 014304 (2020).
[42] P. Chu, Y. Zhou, Y. Jiang, H. Ma, H. Liu, X. Zhang, and X. Li, Eur. Phys. J. C **81**, 93 (2021).
[43] P. Möller, J. R. Nix, W. D. Myers, and W. J. Swiatecki, At. Data Nucl. Data Tables **59**, 185 (1995).
[44] Y. Aboussir, J. M. Pearson, A. K. Dutta, and F. Tondeur, At. Data Nucl. Data Tables **61**, 127 (1995).
[45] S. Raman, C. W. Nestor Jr., and P. Tikkanen, At. Data Nucl. Data Tables **78**, 1 (2001).
[46] E. Moya de Guerra, Ann. Phys. (NY) **128**, 286 (1980).
[47] E. Moya de Guerra, Phys. Rep. **138**, 293 (1986).
[48] T. Liang, J. Liu, Z. Ren, C. Xu, and S. Wang, Phys. Rev. C **98**, 044310 (2018).
[49] L. Wang, J. Liu, T. Liang, Z. Ren, C. Xu, and S. Wang, J. Phys. G **47**, 025105 (2020).
[50] D. B. Day, J. S. McCarthy, T. W. Donnelly, and I. Sick, Annu. Rev. Nucl. Part. Sci. **40**, 357 (1990).
[51] O. Benhar, D. Day, and I. Sick, Rev. Mod. Phys. **80**, 189 (2008).
[52] J. Arrington, D. W. Higinbotham, G. Rosner, and M. Sargsian, Prog. Part. Nucl. Phys. **67**, 898 (2012).
[53] C. Ciofi degli Atti, Phys. Rep. **590**, 1 (2015).
[54] O. Benhar, P. Huber, C. Mariani, and D. Meloni, Phys. Rep. **700**, 1 (2017).
[55] I. Sick, Prog. Part. Nucl. Phys. **47**, 245 (2001).
[56] T. W. Donnelly and J. D. Walecka, Annu. Rev. Nucl. Part. Sci. **25**, 329 (1975).
[57] V. Pascalutsa, M. Vanderhaeghen, and S. N. Yang, Phys. Rep. **437**, 125 (2007).
[58] J. I. Friedman and H. W. Kendall, Annu. Rev. Nucl. Part. Sci. **22**, 203 (1972).
[59] C. Ciofi degli Atti, E. Pace, and G. Salmè, Phys. Rev. C **43**, 1155 (1991).
[60] C. Ciofi degli Atti and S. Simula, Phys. Rev. C **53**, 1689 (1996).
[61] N. Fomin *et al.*, Phys. Rev. Lett. **108**, 092502 (2012).
[62] W. M. Alberico, A. Molinari, T. W. Donnelly, E. L. Kronenberg, and J. W. Van Orden, Phys. Rev. C **38**, 1801 (1988).
[63] A. N. Antonov, P. E. Hodgson, and I. Z. Petkov, *Nucleon Correlations in Nuclei* (Springer, Berlin, 1993).
[64] A. N. Antonov, M. K. Gaidarov, D. N. Kadrev, M. V. Ivanov, E. M. de Guerra, and J. M. Udias, Phys. Rev. C **69**, 044321 (2004).
[65] A. N. Antonov, M. K. Gaidarov, M. V. Ivanov, D. N. Kadrev, E. Moya de Guerra, P. Sarriguren, and J. M. Udias, Phys. Rev. C **71**, 014317 (2005).
[66] J. A. Maruhn, M. Kimura, S. Schramm, P.-G. Reinhard, H. Horiuchi, and A. Tohsaki, Phys. Rev. C **74**, 044311 (2006).
[67] J. Okołowicz, M. Płoszajczak, and W. Nazarewicz, Prog. Theor. Phys. Suppl. **196**, 230 (2012).
[68] P. Sarriguren, D. Merino, O. Moreno, E. Moya de Guerra, D. N. Kadrev, A. N. Antonov, and M. K. Gaidarov, Phys. Rev. C **99**, 034325 (2019).
[69] B. Hernández, P. Sarriguren, O. Moreno, E. Moya de Guerra, D. N. Kadrev, and A. N. Antonov, Phys. Rev. C **103**, 014303 (2021).
[70] G. A. Lalazissis, T. Nikšić, D. Vretenar, and P. Ring, Phys. Rev. C **71**, 024312 (2005).
[71] E. Moya de Guerra, P. Sarriguren, J. A. Caballero, M. Casas, and D. W. L. Sprung, Nucl. Phys. A **529**, 68 (1991).
[72] A. N. Antonov, M. V. Ivanov, M. K. Gaidarov, E. Moya de Guerra, J. A. Caballero, M. B. Barbaro, J. M. Udias, and P. Sarriguren, Phys. Rev. C **74**, 054603 (2006).
[73] C. Maieron, T. W. Donnelly, and I. Sick, Phys. Rev. C **65**, 025502 (2002).
[74] J. E. Amaro, M. B. Barbaro, J. A. Caballero, T. W. Donnelly, A. Molinari, and I. Sick, Phys. Rev. C **71**, 015501 (2005).
[75] J. E. Amaro, M. B. Barbaro, J. A. Caballero, T. W. Donnelly, and A. Molinari, Nucl. Phys. A **657**, 161 (1999).
[76] T. Nikšić, D. Vretenar, P. Finelli, and P. Ring, Phys. Rev. C **66**, 024306 (2002).
[77] I. Sick and J. S. McCarthy, Nucl. Phys. A **150**, 631 (1970).
[78] A. Meucci, M. Vorabbi, C. Giusti, F. D. Pacati, and P. Finelli, Phys. Rev. C **87**, 054620 (2013).
[79] J.-L. Basdevant, J. Rich, and M. Spiro, *Fundamentals in Nuclear Physics: From Nuclear Structure to Cosmology* (Springer, New York, 2005).
[80] R. M. Sealock, K. L. Giovanetti, S. T. Thornton, Z. E. Meziani, O. A. Rondon-Aramayo, S. Auffret, J.-P. Chen, D. G. Christian, D. B. Day, J. S. McCarthy, R. C. Minehart, L. C. Dennis, K. W. Kemper, B. A. Mecking, and J. Morgenstern, Phys. Rev. Lett. **62**, 1350 (1989).
[81] H. Nakamura, T. Nasu, M. Sakuda, and O. Benhar, Phys. Rev. C **76**, 065208 (2007).
[82] E. A. Knight, R. P. Singhal, R. G. Arthur, and M. W. S. Macauley, J. Phys. G **7**, 1115 (1981).